Astronomical and Astrophysical Transactions (*AApTr*), 2025, Vol. 35, Issue 4, pp. 431–438,
ISSN 1055-6796, Photocopying permitted by license only, ©Cambridge Scientific Publishers

Comparative study of chemistry in massive star-forming regions S255IR and NGC7538C

P.A. Tanatova[1,*], S.V. Salii[2]

[1] *Ural Federal University, Department of Astronomy, Geodesy, Ecology and Environmental Monitoring, 48 Kuibyshev Street, Ekaterinburg, 620026 Russia*
[2] *Kourovka Astronomical Observatory, 1 Observatory Street, Sloboda Village, District Pervouralsk, Sverdlovsk Region, 623132 Russia*

Received 15 June, 2025; accepted 26 August, 2025

In this work, we examined the chemical composition of the S255IR and NGC 7538C regions. In the S255IR source, we identified 18 molecules and isotopologues, while in the NGC 7538C source, we detected 16, ranging from simple diatomic species (e.g., CO) to complex six-atom molecules (e.g., CH_3CN and CH_3OH). We constructed the velocity distribution of emission for various molecules. Based on our findings, we suggest that the NGC 7538C source is at an earlier evolutionary stage compared to S255IR.

Assuming local thermodynamic equilibrium (LTE), we estimated the rotational temperatures by some observed molecules (143–166 K for S255IR and from 69 to 417 K for NGC 7538C). The significant difference in temperature within the NGC 7538C may be due to the presence of two thermal regions within this object. Additionally, we derived the column densities of observed molecules for both objects.

Keywords: Stars: massive – galaxies: star formation – ISM: molecules – ISM: individual objects (S255IR, NGC 7538C)

1 Introduction

The processes of massive star formation remain less studied compared to the mechanisms of low-mass star formation. This is due to a number of observational challenges: short evolutionary timescales of massive star-forming regions, in the order of 10^4 years (Churchwell 2002), and the fact that in the early stages of evolution, massive stars are completely embedded within their parent molecular clouds, making direct observations difficult (Kurtz et al. 2000). Analyzing the physical and chemical properties of massive star-forming regions at different evolutionary stages is crucial for understanding the formation mechanisms and early evolution of massive stars. Meanwhile, the study of molecular spectra serves as a powerful tool for assessing the physical conditions and kinematic properties of these objects.

*Email: Polina.Fedina@urfu.me

For our investigation, we selected the S255IR and NGC 7538C sources. Both objects exhibit a rich diversity of molecular lines, which enables us not only to study each source in detail but also to perform a comparative analysis that reveals key differences in physical conditions and chemical composition at different stages of massive star formation. It is important to note that the observations of both objects were carried out within a single observing project using the same telescope, which ensures data consistency and enables their direct and unambiguous comparison. The aim of this study was to determine and compare the physical conditions in two massive star-forming regions through analysis of their molecular spectra, as well as to examine molecular markers of different physical states.

S255IR (G192.600–0.048) is a well-studied massive star-forming region at a distance of 1.78 kpc (Burns et al. 2016), forming part of a known massive star-forming complex located between the HII regions (Sharpless S. 1959) S255 and S257. The S255IR region contains a cluster of B-class stars (Howard et al. 1997, Itoh et al. 2001), compact HII regions (Snell & Bally 1986), numerous HII emission zones (Miralles et al. 1997), collimated high-velocity outflows (Wang et al. 2011), as well as H_2O and CH_3OH masers (Burns et al. 2016, Salii et al. 2019), all indicating active ongoing star formation processes in this region.

The object NGC 7538C (G111.542+0.776, NGC 7538 IRS 1) is an active massive star-forming region located at a distance of 2.65 kpc (Moscadelli et al. 2009). This object represents a rich source of maser emission, where hydroxyl (OH), water (H_2O), ammonia (NH_3), methanol (CH_3OH), and formaldehyde (H_2CO) masers have been detected (Gaume et al. 1991, Hutawarakorn & Cohen 2003, Hoffman et al. 2003, Kurtz et al. 2004). Outflows have been observed in this region (Moscadelli et al. 2025), which, together with the maser emission from this area, indicates active ongoing star formation.

2 Observation

This work makes use of observations of S255IR and NGC 7538C conducted in January 2019 using the IRAM 30-m as part of project 155-18 (PI: Igor Zinchenko). Telescope equipped with the EMIR receiver across four frequency bands: 326.7–330.7 GHz, 329.5–334.5 GHz, 342.4–346.4 GHz, and 346.1–350.2 GHz. At these frequencies, the beam size and spectral resolution are $7.5''$ and ~ 1.4 km/s, respectively. The spectra were obtained at coordinates $\alpha_{2000} = 06^{\rm h}12^{\rm m}54.015^{\rm s}$, $\delta_{2000} = +17°59'23.05''$ for S255IR and $\alpha_{2000} = 23^{\rm h}13^{\rm m}45.386^{\rm s}$, $\delta_{2000} = +61°28'9.81''$ for NGC 7538C (Salii et al. 2019).

3 Results

3.1 Molecular line identification

The spectral line identification was performed using the CLASS software from the GILDAS package (http://www.iram.fr/IRAMFR/GILDAS). The transition parameters were obtained from the CDMS catalog (Müller et al. 2001, 2005; https://cdms.

astro.uni-koeln.de/cdms/portal), considering only transitions with upper level energies below 1000 K, as no transitions with higher energies were identified.

We detected emission lines from 18 molecules and their isotopologues toward the S255IR region and 16 toward the NGC 7538C region, all transitions with intensities above the 3σ threshold are listed in Table 1. The spectral transitions of various molecules serve as indicators of physical processes occurring in the system. Typically, hot cores are identified by rotational transitions of complex organic molecules (CH_3OH, HCOOH, H_2CS, CH_3CN, see, e.g., Bisschop et al. 2007). Dense cores are characterized by molecules with high dipole moments (CS, HC_3N, see, e.g., Chapman et al. 2009). The most likely molecules in outflows are those evaporated from dust grain mantles (SO, ^{33}SO, SO_2, see, e.g., Charnley 1997).

Both regions exhibit a similar chemical inventory, with tracers of dense gas, hot cores, and outflows detected in each (Table 1).

S255IR: In this region, we observed transitions of SO, ^{33}SO, and SO_2 with high quantum numbers (8–7, 9–8), which trace high-velocity, collimated outflows. Additionally, we detected emission from molecules that serve as tracers of dense cores (HC_3N) and hot cores (CH_3OH, HCOOH, H_2CS).

NGC 7538C: In this region, we identified spectral lines of hot core tracer molecules (CH_3OH, HNCO, HCOOH, H_2CS). However, lines from molecules associated with high-velocity outflows are weak (<0.1 K at 5σ) or completely absent, as are molecules tracing dense cores.

Table 1 The tabular parameters for each transition include: rest frequency, quantum numbers, and upper energy level. Plus signs (+) mark transitions identified above the 3σ threshold.

Molecule	Frequency (GHz)	Transition	E_{up} (K)	S255IR	NGC 7538C
CO	345.796	3–2	33.2	+	+
^{13}CO	330.588	3–2	31.7	+	+
$C^{18}O$	329.331	3–2	31.6	+	+
SO	329.385	2_1–1_0	15.8	+	–
	344.311	8_8–7_7	87.5	+	+
	346.528	8_9–7_8	78.8	–	+
^{33}SO	343.086	9_8–8_7	78.1	+	–
SiO	347.331	8–7	75.0	+	+
CS	342.883	7_0–6_0	65.8	+	+
NS	346.220	$8_{1,8}$–$7_{1,7}$	69.8	+	+
SO_2	326.867	$20_{4,16}$–$20_{3,17}$	232.9	+	–
	332.505	$4_{3,1}$–$3_{2,2}$	31.3	+	+
	342.761	34_3–34_2	581.9	+	–
	345.339	$13_{2,12}$–$12_{1,11}$	92.9	+	+
	346.652	$19_{1,19}$–$18_{0,18}$	168.1	+	+
CCH	349.338	$4_{5,5}$–$3_{4,4}$	41.9	+	+
OCS	328.298	27–26	220.6	+	+
$HC^{15}N$	344.200	4–3	41.3	+	+
H_2CS	342.944	$10_{0,10}$–$9_{0,9}$	90.6	+	+
	343.322	$10_{2,9}$–$9_{2,8}$	143.3	+	+

Molecule	Frequency (GHz)	Transition	E_{up} (K)	S255IR	NGC 7538C
	343.409	$10_{3,8}$–$9_{3,7}$	209.1	+	–
	343.414	$10_{3,7}$–$9_{3,6}$	209.1	+	+
HNCO	329.460	$15_{3,13}$–$14_{3,12}$	501.5	–	+
	329.573	$15_{2,14}$–$14_{2,13}$	296.8	–	+
	329.664	$15_{0,15}$–$14_{0,14}$	126.6	+	+
HCOOH	334.266	$15_{2,14}$–$14_{2,13}$	141.6	+	+
	342.521	$16_{1,16}$–$15_{1,15}$	143.6	+	+
	343.952	$15_{1,14}$–$14_{1,13}$	136.3	+	+
	345.031	$16_{0,16}$–$15_{0,15}$	143.1	+	+
HC_3N	345.609	38–37	41.3	+	–
CH_3CN	330.760	$18_{7,0}$–$17_{7,0}$	500.7	+	+
	330.843	$18_{6,0}$–$17_{6,0}$	407.9	+	+
	330.913	$18_{5,0}$–$17_{5,0}$	329.5	+	+
	330.970	$18_{4,0}$–$17_{4,0}$	265.2	+	+
	331.014	$18_{3,0}$–$17_{3,0}$	215.2	+	+
	331.046	$18_{2,0}$–$17_{2,0}$	179.5	+	+
	331.065	$18_{1,0}$–$17_{1,0}$	158.1	+	+
	331.072	$18_{0,0}$–$17_{0,0}$	151.0	+	+
	349.125	$19_{7,0}$–$18_{7,0}$	517.4	+	+
	349.212	$19_{6,0}$–$18_{6,0}$	424.7	+	+
	349.286	$19_{5,0}$–$18_{5,0}$	346.2	+	+
	349.346	$19_{4,0}$–$18_{4,0}$	281.9	+	–
	349.393	$19_{3,0}$–$18_{3,0}$	232.0	+	–
	349.427	$19_{2,0}$–$18_{2,0}$	196.3	+	+
	349.447	$19_{1,0}$–$18_{1,0}$	174.9	+	+
	349.454	$19_{0,0}$–$18_{0,0}$	167.7	+	+
CH_3OH	326.961	$10_{1,10}$–$9_{0,9}$	133.1	+	+
	327.317	$12_{2,11}$–$11_{3,8}$	218.7	–	+
	327.441	$17_{5,12}$–$18_{4,15}$	492.8	–	+
	327.487	$13_{4,9}$–$14_{3,12}$	307.2	+	+
	329.633	$12_{2,10}$–$11_{3,9}$	218.8	+	+
	330.794	$8_{3,5}$–$9_{2,7}$	146.3	+	+
	331.072	$12_{3,9}$–$11_{5,7}$	597.8	–	+
	331.220	$16_{1,16}$–$15_{2,13}$	320.6	+	+
	331.502	$11_{1,10}$–$11_{0,11}$	169.0	+	+
	332.997	$22_{2,20}$–$21_{3,18}$	614.5	–	+
	334.427	$3_{0,3}$–$2_{1,2}$	314.5	+	+
	342.730	$13_{1,12}$–$13_{0,13}$	227.5	+	+
	344.109	$8_{2,17}$–$17_{3,15}$	419.4	+	+
	344.443	$19_{1,19}$–$18_{2,16}$	451.2	+	+
	345.904	$16_{1,15}$–$15_{2,14}$	332.7	+	+
	345.919	$18_{3,15}$–$17_{4,14}$	459.4	+	+
	346.203	$5_{4,2}$–$6_{3,3}$	115.2	+	+
	346.204	$5_{4,1}$–$6_{3,4}$	115.2	+	+
	349.107	$14_{1,13}$–$14_{0,14}$	260.2	+	+

3.2 Chemical differentiation

For both objects, we constructed the velocity distributions of molecular emission (Fig. 1). The systemic velocity of the S255IR source is ∼5 km/s (Fujisawa et al. 2015), but emission is observed across velocities from ∼2 to ∼8 km/s, indicating a chemically inhomogeneous object with complex structure (Zinchenko et al. 2020, 2024) where molecules observed at different velocities may originate from distinct regions of the source. The emission from outflow-tracing molecules appears at ∼7.7± 0.6 km/s, corresponding to the systemic velocities of the SMA1 and SMA2 clumps. Molecules serving as hot core and dense core tracers exhibit velocities close to the systemic velocity of ∼5±1 km/s.

The systemic velocity of NGC 7538C is ∼–58.56 km/s, with observed emission spanning velocities of methanol maser from ∼–62 km/s to ∼–48 km/s (Pestalozzi, Minier & Booth 2005). Based on our analysis, simple molecules in this region are also detected at higher velocities of ∼–57±0.2 km/s, while more complex molecules are typically observed at average velocities of ∼–59.3±0.5 km/s. In this source, emission from three protostars is observed, with velocities of the two most massive being ∼–59.5 km/s and ∼–56.4 km/s (Goddi et al. 2015), these velocities correspond to the velocities we determined for complex and simple molecules, respectively.

This velocity distribution pattern in both objects reveals a complex chemical structure that cannot be attributed to measurement uncertainties, since the radial velocity differences significantly exceed the 1.4 km/s spectral resolution of our observations.

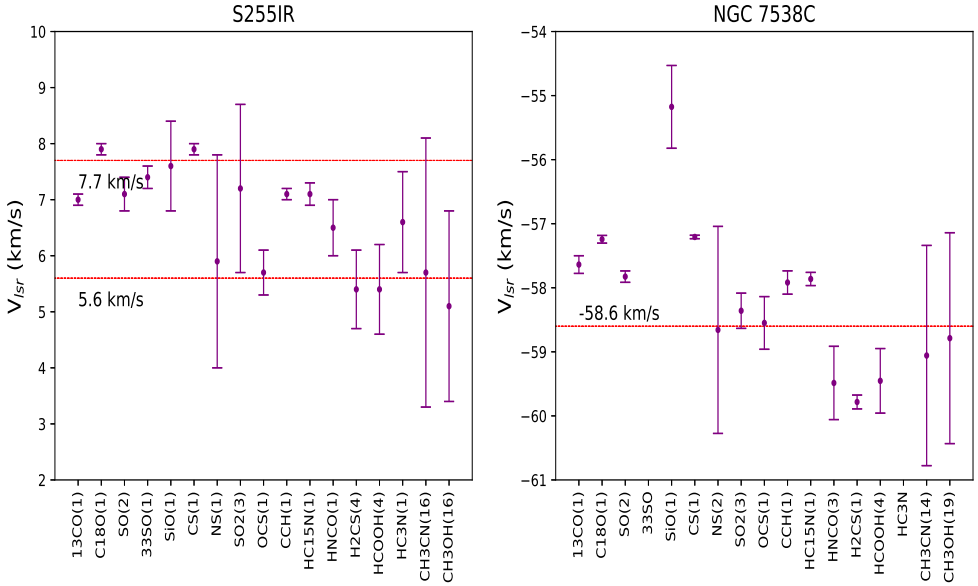


Figure 1 Velocity distribution of emission. The number of identified lines is indicated in parentheses, and the red line corresponds to the systemic velocity of the object and of SMA1 and SMA2 clumps for S255IR and systemic velocity of the object for NGC 7538C. The error bar shows the total error in determining the velocities for all lines of one molecule.

3.3 Rotational temperatures and column densities of observed molecules

For five molecular species, we successfully identified three or more spectral lines and derived estimates of temperatures and column densities of observed molecules using the rotational diagram method (Kalenskii & Kurtz 2016). This method assumes optically thin lines and LTE. Rotational diagrams were constructed using lines with intensities above 3σ, our derived parameters are presented in Table 2. Lines with optical thickness $\tau < 1$ were used for the analysis.

We obtained rotational temperatures for the S255IR region ranging from 143±30 K for CH_3CN to 166 ± 65 K for CH_3OH, with column densities. Our temperature estimates derived from different molecules agree within the error margins and are characteristic of a hot core environment.

Table 2 Rotational temperatures ($T_{\rm rot}$), column densities ($N_{\rm rot}$) of observed molecules in S255IR and NGC 7538C regions.

	S255IR		NGC 7538C	
Molecule	$N_{\rm rot}$ (cm^{-2})	$T_{\rm rot}$ (K)	$N_{\rm rot}$ (cm^{-2})	$T_{\rm rot}$ (K)
SO_2	$(5 \pm 1)\times10^{14}$	145 ± 65	$(5 \pm 1)\times10^{12}$	69 ± 35
H_2CS	$(7 \pm 4)\times10^{14}$	149 ± 100	–	–
CH_3OH	$(3 \pm 1)\times10^{15}$	166 ± 65	$(1 \pm 0.7)\times10^{12}$	149 ± 50
CH_3CN	$(3 \pm 1)\times10^{13}$	143 ± 30	$(6 \pm 1)\times10^{11}$	417 ± 45

The derived rotational temperatures for the NGC 7538C source span a broad range from 69±35 K for SO_2 to 417±45 K for CH_3CN, this indicates chemical fractionation where SO_2 may emit from colder regions, for example from outflows, while CH_3OH and CH_3CN emit from the hot core region. The temperature differences among hot core tracers suggest the presence of two thermal regions in this object, consistent with Knez et al. 2003. Their TEXES infrared telescope observations of HCN and C_2H_2 were reproduced by astrochemical modeling, the cold component exhibits a temperature of ∼110 K, while the hot component reaches ∼685 K. In the work by Goddi et al. 2015, on differences in velocities and densities of NH_3 emission regions from JVLA interferometer observations, it was found that NGC 7538C is a complex system of three protostars in an extended envelope, this may also explain such differences in our rotational temperature estimates, CH_3CN lines are more optically thin and presumably emit from deeper core regions compared to CH_3OH lines.

Column densities for the source NGC 7538C are notably lower than those obtained for the S255IR region, The difference in the estimated column densities of the molecules under consideration is consistent with the difference in the hydrogen column densities, N(H_2)=9.7×10^{24} cm^{-2} for S255IR (Liu et al. 2020) and N(H_2)=1.6×10^{22} cm^{-2} for NGC 7538C (Jacob et al. 2022).

3.4 Molecular tracers of evolutionary staging

As is known, different physical conditions are required for the formation of various molecules. In star-forming regions, we can observe molecules that are associated with dense matter, hot cores, and outflows. Younger massive star-forming regions typically exhibit maser activity, lower core densities, and less collimated low-velocity outflows.

Consequently, such cores show fewer outflow-tracing and dense-core tracer molecules, lines with lower upper-level energy, and generally lower column densities (Zinnecker & Harold 2007, Motte et al. 2018).

The S255IR object displays numerous intense lines from outflow-tracing molecules, whereas NGC 7538C shows weak or absent emission from these species, it is also important to note that only lines with lower upper-level (93 K for SO_2) energies are observed for these molecules. A certain dense-core tracer molecule (HC_3N) is also undetected in NGC 7538C. Furthermore, the observed gas column densities in NGC 7538C are significantly lower compared to S255IR. The combination of these factors may be explained by differences in the stages of evolution of the regions. However, despite these physical differences, we emphasize that evolutionary boundaries in star formation processes remain poorly defined, making clear classification challenging.

4 Conclusions

We identified emission lines from 18 molecular species toward the S255IR region and 16 toward NGC 7538C. The analysis revealed chemical fractionation in both sources, which is driven predominantly by kinematics in S255IR, but by a combination of kinematics and, to a greater extent, temperature gradients in NGC 7538C. Using the rotational diagram method, we determined column densities of observed molecules and temperatures for both sources. For NGC 7538C, we tentatively identified emission originating from two thermal regions. Based on the emission from tracer molecules characteristic of different physical conditions and our derived column densities, we conclude that NGC 7538C is at an earlier evolutionary stage compared to S255IR.

Acknowledgements

We thank the reviewer for their valuable comments on our article, which have contributed to a better understanding of our work.

This work is based on observations carried out under project number 155-18 with the IRAM 30m telescope. IRAM is supported by INSU/CNRS (France), MPG (Germany) and IGN (Spain).

This research was supported by the Ministry of Science and Higher Education of the Russian Federation, research project FEUZ-2023-0019.

References

Bisschop S.E., Jørgensen J.K., van Dishoeck E.F. et al. (2007) A&A 465, 913
Burns R. A., Handa T., Nagayama T., et al. (2016) MNRAS 460, 283
Charnley S.B. (1997) ApJ 481, 396
Churchwell E. (2002) The Formation and Early Evolution of Massive Stars/Hot Star Workshop III: The Earliest Phases of Massive Star Birth, 3

Chapman J.F., Millar T.J., Wardle M. et al. (2009) MNRAS 394, 221
Fujisawa K., Yonekura Y., Sugiyama K. et al. (2015) Astron. Telegram, 8286, 1
Gaume R.A., Johnston K.J., Nguyen H.A. et al. (1991) ApJ 376, 608
Goddi C., Zhang Q., Moscadelli L. (2015) Astron. Astrophys., 573, A108
Hoffman I.M., Goss W.M., Palmer P. et al. (2003) ApJ 598, 1061
Howard, E. M., Pipher, J. L., Forrest, W. J. (1997) ApJ 481, 327
Hutawarakorn B., Cohen R.J. (2003) MNRAS 345, 175
Itoh, Y., Tamura, M., Suto, H., et al. (2001) PASJ 53, 495
Jacob A.M., Neufeld D.A., Schilke P. et al. (2022) ApJ 930, 141
Kalenskii S.V., Kurtz S. (2016) Astronomy Reports 60, 702-717
Knez C., Lacy J.H., Evans N.J. et al. (2003) The Study of Interstellar Chemistry through Mid-Infrared Spectroscopy/Revista Mexicana de Astronomia y Astrofisica Conference Series, 45
Kurtz S., Cesaroni R., Churchwell E., et al. (2000) Hot Molecular Cores and the Earliest Phases of High-Mass Star Formation/Protostars and Planets IV, 299
Kurtz S., Hofner P., Álvarez C.V. (2004) ApJS 155, 149
Liu S.-Y., Su Y.-N., Zinchenko I. et al. (2020) ApJ 904, 181
Miralles, M. P., Salas, L., Cruz-Gonzalez, I., Kurtz, S. (1997) ApJ 488, 749
Müller, H. S. P., Thorwirth, S., Roth, D. A., & Winnewisser, G. (2001) A&A 370, L49
Müller, H. S. P., Schlöder, F., Stutzki, J., Winnewisser, G. (2005) JMoSt 742, 215
Moscadelli L., Reid M.J., Menten K.M. et al. (2009) ApJ 693, 406
Motte F., Bontemps S., Louvet F. (2018) ARA&A 56, 41
Pestalozzi M. R., Minier V., Booth R. S. (2005) A&A 432, 737
Sharpless S. (1959) ApJS, 4, 257
Snell, R. L., Bally, J. (1986) ApJ 303, 683
Salii S.V., Zinchenko I.I., Liu S.-Y. et al. (2022) MNRAS 512, 3215
Wang, Y., Beuther, H., Bik, A., et al. (2011) A&A 527, A32
Zinnecker H., Yorke H.W. (2007) ARA&A 45, 481
Zinchenko I.I., Liu S.-Y., Su Y.-N. et al. (2020) Astrophys. J., 889, 43
Zinchenko I.I., Liu S.-Y., Su Y.-N. (2024) Astron. Astrophys., 692, A181